

Vortices in a thin film superconductor with a spherical geometry

M. J. W. Dodgson and M. A. Moore

Theoretical Physics Group

Department of Physics and Astronomy

The University of Manchester, M13 9PL, UK

(June 7, 1996)

We report results from Monte Carlo simulations of a thin film superconductor in a spherical geometry within the lowest Landau level approximation. We observe the absence of a phase transition to a low temperature vortex solid phase with these boundary conditions; the system remains in the vortex liquid phase for all accessible temperatures. The correlation lengths are measured for phase coherence and density modulation. Both lengths display identical temperature dependences, with an asymptotic scaling form consistent with a continuous zero temperature transition. This contrasts with the first order freezing transition which is seen in the alternative quasi-periodic boundary conditions. The high temperature perturbation theory and the ground states of the spherical system suggest that the thermodynamic limit of the spherical geometry is the same as that on the flat plane. We discuss the advantages and drawbacks of simulations with different geometries, and compare with current experimental conclusions. The effect of having a large scale inhomogeneity in the applied field is also considered.

74.20.De, 74.76-w

I. INTRODUCTION

The existence and nature of melting transitions in two-dimensional (2D) systems remains a topic of interest and uncertainty in both theory and experiments. In particular, the melting of the vortex lattice in a thin film superconductor has received much attention. A continuous melting transition from an Abrikosov lattice to a vortex liquid via a phase of hexatic order, as in the Kosterlitz-Thouless-Halperin-Nelson-Young (KTHNY) theory, was first proposed over fifteen years ago.¹ A “transition” in the current-voltage response of thin film superconductors has been seen in several experiments.²⁻⁴ The vortex system becomes depinned above some transition temperature (the depinned vortices will dissipate energy as they move, leading to an Ohmic response) and the rise of the resistivity of the film is presumed to be caused by the melting of the vortex lattice. However, it seems that this transition temperature varies with the strength of the pinning centers in the thin films. For films of amorphous NbO the pinning is weak and no features can be detected in the current-voltage characteristics which may be attributed to a “transition”. This has been interpreted as being due to the absence of the Abrikosov vortex lattice.⁵

The superconducting state arises from macroscopic correlations in the phase of the Cooper pair wave function, or equivalently the Ginzburg-Landau order parameter. This phase coherence is usually a consequence of off-diagonal long range order (ODLRO), i.e. non-vanishing $\langle \psi \rangle$, where ψ is the superconducting order parameter. It has been predicted that thermal excitations of the shear modes of the vortex lattice should destroy ODLRO in the crystalline state and the length scale over which phase coherence persists has been estimated.^{6,7}

O’Neill and Moore have performed Monte Carlo (MC)

simulations of thin film superconductors within the lowest Landau level (LLL) approximation using a spherical geometry to minimize finite size boundary effects.⁷ No freezing transition out of the vortex liquid phase was found in the temperature region investigated. The correlation function associated with the positions of the vortices was calculated and the associated length scale of these lattice-like correlations was found to diverge only in the zero temperature limit. It was noted that this happened on a similar length scale over which there was expected to be phase coherence from the arguments of Refs. 6 and 7.

In the work of O’Neill and Moore, the superconducting film existed on the surface of a sphere, and this geometry is the one employed here. The magnetic field perpendicular to the surface is generated by a magnetic monopole placed at the center of the sphere.⁸ The strength of the monopole must be quantized to have a well defined superconducting order parameter, but the strength of the field at the surface may be continuously varied by changing the radius of the sphere. The LLL approximation, which assumes an infinite magnetic screening length, works well in the 2D case where the effective screening length is $\Lambda_{eff} = 2\lambda^2/d$ because of the magnetic field outside the superconductor.⁹ Λ_{eff} becomes large as the film thickness d is reduced; λ is the bulk magnetic penetration length. It is often the case that Λ_{eff} is greater than the film dimensions for small d .

More recently, strong evidence for a first order transition at a finite temperature in an alternative finite size approximation with quasi-periodic boundary conditions (QP) on an infinite plane has come from MC simulations.¹⁰⁻¹⁴ This model has a periodic amplitude of the order parameter and a fixed change in the phase as a unit cell containing N vortices is crossed (the change

in phase depends on the choice of gauge). The quasi-periodicity in the phase places some constraints on the motion of the vortices, but it is not obvious that this will change the thermodynamic properties of the system. The observed transition temperature is within the range investigated on the sphere. This raises the question of whether or not there really is no transition on the sphere. If so, then what are the reasons that different boundary conditions give different results?

If there is a freezing transition, at least on the plane, does this contradict the theoretical prediction of no ODLRO at finite temperatures? Apparently not, as the work of Sasik, Stroud and Tesanovic¹⁴ (SST) has concluded that in the thermodynamic limit even the low temperature state below the first order transition has no ODLRO, despite the presence of “Bragg peaks” in the correlations of the order parameter density (the peaks will not be delta-functions but the algebraic singularities expected for a 2D crystalline system¹⁵). These conclusions of SST are taken as support for the “charge-density wave” phase (with a modulation in the Cooper pair density, but no ODLRO) proposed by Tesanovic.¹⁶

In this work we again fail to find a phase transition in the spherical geometry. We have investigated the correlations associated with both the *phase* and the *amplitude* of the superconducting order parameter. One advantage of the spherical geometry is that the liquid state may be investigated over a larger range of temperatures. This has allowed us to compare the growing length scales of the phase and amplitude correlations over a large variation in temperature.

Section II contains the formulation of our model. In section III it is shown how the high temperature perturbation theory on the spherical geometry gives the same free energy per vortex as the conventional theory in the thermodynamic limit. In Section IV we describe how the ground state of the vortex system on the sphere is affected by the necessity of containing twelve disclination defects within the triangular lattice. We have previously concluded that these defects with long range strains will give a finite energy cost per vortex relative to the flat plane ground state even in the thermodynamic limit.¹⁷ However, the presence of dislocation defects were not considered, and these can screen the strains of the disclinations to recover the thermodynamic limit of the triangular lattice on a flat plane. This screening is described in the framework of elasticity theory, and the numerical evidence for dislocations in the ground state is reexamined. In Section VA our calculations on the four-point density correlation function of the vortex liquid are shown. This is followed by our investigations on the phase coherence in Section VB.

The spherical geometry is in principle realizable using the end of a long thin solenoid to approximate the field from a monopole and placing it inside a spherical superconducting film. However there would always be a problem in the placement of the solenoid which would lead to a large scale inhomogeneity in the field strength at the

spherical surface. Additional simulations are described in Section VI, where we add just such an inhomogeneous magnetic field.

Finally, in the light of different conclusions from simulations of the LLL system in different geometries, we discuss some of the problems in these geometries in Section VII and comment on the experimental situation. Some conclusions are drawn in Section VIII.

II. DESCRIPTION OF THE MODEL

We model a thin film superconductor by a spherical shell of radius R and thickness $d \ll R$. An external magnetic field $\mathbf{H}(\mathbf{r}) = \hat{\mathbf{r}}H(r)$, always directed perpendicular to the shell’s surface is created by a magnetic monopole at the center of the sphere. We neglect all fluctuations in the magnetic induction so that it always has the mean value $B = \mu_0 H(R)$ on the superconducting surface. Dirac’s quantization condition⁸ (assuming that the basic unit of charge is that of a Cooper pair) requires that the total flux through the surface is an integer multiple of flux quanta $N\hbar/2e$. Our choice of gauge that satisfies $\nabla \times \mathbf{A} = \mathbf{B}$ is $\mathbf{A} \equiv (A_r, A_\theta, A_\phi) = (0, 0, BR \tan \theta/2)$. We also assume that the superconductor is described by a Ginzburg-Landau (GL) complex order parameter ψ with a phenomenological free energy Hamiltonian given by

$$\mathcal{H}[\psi] = \int d^3r \left[\alpha(T)|\psi|^2 + \frac{\beta}{2}|\psi|^4 + \frac{1}{2m}\psi^*D^2\psi \right], \quad (2.1)$$

where $D^2 = \mathbf{D} \cdot \mathbf{D}$ and $\mathbf{D} = -i\hbar\nabla - 2e\mathbf{A}$ is the gauge invariant derivative operator. The LLL approximation consists in expanding this order parameter in terms of the eigenstates of D^2 , and then only keeping the degenerate level of states with the lowest eigenvalue. If we only consider the two dimensions on the surface of the sphere then the subspace of this LLL is spanned by $N + 1$ orthonormal functions:¹⁸

$$\psi_m(\theta, \phi) = h_m e^{im\phi} \sin^m(\theta/2) \cos^{N-m}(\theta/2), \quad (2.2)$$

with $m = 0, \dots, N$ and $h_m = [(N + 1)!/4\pi R^2 m!(N - m)!]^{1/2}$. We write the order parameter as $\psi(\theta, \phi) = Q \sum v_m \psi_m(\theta, \phi)$ with $Q = (\Phi_0 k_B T / \beta d B)^{1/4}$, and measure lengths in units of the magnetic length $l_m = (\Phi_0/2\pi B)^{1/2}$ which fixes $R = (N/2)^{1/2}$. [Note that the lattice spacing l_0 in a triangular vortex lattice will be given by $l_0 = (4\pi/\sqrt{3})^{1/2} l_m \simeq 2.69 l_m$.] The LLL Hamiltonian can then be written as

$$\begin{aligned} \mathcal{H}(\{u_m\}) = k_B T \alpha_T^2 \times & \quad (2.3) \\ \left[\text{sgn}(\alpha_T) \sum_{m=0}^N u_m u_m^* + \sum_{p,q,r,s=0}^N w_{pqrs} u_p u_q u_r^* u_s^* \delta_{p+q,r+s} \right], \end{aligned}$$

with $u_m = v_m / |\alpha_T|^{1/2}$. The quartic coupling term is given by⁷

$$w_{pqrs} = \frac{(N+1)^2}{2N(2N+1)} f_{pq} f_{rs}, \quad (2.4)$$

where $f_{pq}^2 = C_p^N C_q^N / C_{p+q}^{2N}$ and $C_i^j = j!/[i!(j-i)!]$ is the binomial coefficient.

Our effective reduced temperature variable is

$$\alpha_T = \frac{dQ^2}{k_B T} \left[\alpha(T) + \frac{eB\hbar}{m} \right] = \frac{dQ^2}{k_B T} \alpha' \left[-1 + \frac{T}{T_{c0}} + \frac{H}{H_{c2}(0)} \right]. \quad (2.5)$$

where $\alpha' = T_{c0}(d\alpha/dT)_{T=T_{c0}}$ and T_{c0} is the mean field transition temperature. $H_{c2}(0)$ is the straight line extrapolation to zero temperature of the upper critical field, within mean field theory. For better computational efficiency, Eq. (2.3) maybe rewritten as¹⁹

$$\mathcal{H}(\{u_m\}) = k_B T \alpha_T^2 \left[\text{sgn}(\alpha_T) \sum_{m=0}^N |u_m|^2 + \frac{1}{2N} \sum_{p=0}^{2N} |U_p|^2 \right], \quad (2.6)$$

where $U_p = 2\pi N \sum_{q=0}^N B^{1/2} (2N - p + 1, p + 1) h_q h_{p-q} \Theta(p - q) \Theta(N + q - p) u_q u_{p-q}$ and $B(x, y) = \Gamma(x)\Gamma(y)/\Gamma(x+y)$ is the Beta function. $\Theta(q)$ is the Heaviside step function.

An alternative description of the order parameter on the sphere in the LLL approximation is possible if we write (following Ref. 7) $\psi(\theta, \phi) = Q \sum_{m=0}^N v_m \psi_m(\theta, \phi) = Q \cos^N(\theta/2) \sum_{m=0}^N v_m z^m$, where $z = \tan(\theta/2) e^{i\phi}$. The N th order polynomial may be written as a product of $N+1$ terms to give:

$$\psi(\theta, \phi) = C \cos^N(\theta/2) \prod_{i=1}^N (z - z_i). \quad (2.7)$$

Therefore the order parameter is determined by the positions of the N zeros (vortices) $\{z_i\}$ along with an overall complex amplitude C . It is shown in Appendix A that the GL free energy Hamiltonian depends only on the *relative* positions of these vortices plus the overall complex amplitude, and not on the choice of coordinate system (θ, ϕ) that arose from our choice of gauge. This translational invariance is assumed throughout this paper. Note that there are no constraints on the allowed positions $\{z_i\}$ which is not the case with QP boundary conditions.

The properties of these systems are determined by the partition function $Z = \int \prod_m du_m du_m^* \exp[-\mathcal{H}(\{u_m\})/k_B T]$. We investigate these properties, in particular correlations in the “density” $|\psi|^2$ and the phase $\arg(\psi)$, with the Metropolis algorithm which uses an MC method to sample the phase space.²⁰ We have made measurements for runs up to 10^7 MC steps for system sizes as large as $N = 400$. We have mainly concentrated on the temperature range between $\alpha_T = -2$ and -12 . We have also used standard minimization routines to investigate the ground states of this model.

III. HIGH TEMPERATURE PERTURBATION THEORY ON THE SPHERE

A perturbation expansion has been developed about the Gaussian limit of (2.1) at $\alpha_T \rightarrow +\infty$ to approximate various properties of the LLL system.²¹ In two dimensions the geometry used has always been a flat plane. The series may be represented by Feynman diagrams and many quantities in two and three dimensions have been evaluated to high order.²² The series can extend to negative α_T as long as the propagator is renormalized at least to the level of the Hartree-Fock approximation (HF).

We consider the perturbation series for the free energy using the spherical geometry that leads to the Hamiltonian (2.6). The usual treatment follows for the Feynman diagrams in a ϕ^4 theory, with directed lines representing the gaussian propagator $g_0 = \langle v_p v_p^* \rangle_0$ connecting vertices representing the interaction $\beta_{pqrs} = w_{pqrs} \delta_{p+q, r+s}$, and internal lines are summed from 0 to N . All diagrams with loops are removed by renormalizing the propagator in a self-consistent fashion. This is the HF approximation, and the renormalized propagator, \tilde{g} , must satisfy

$$\tilde{g} = g_0 (1 - 2\tilde{g}^2 S^0), \quad (3.1)$$

where $S^0 = \sum_{q=0}^N \beta_{pqpq}$. On the sphere we find:

$$S_{\text{sphere}}^0 = \frac{N+1}{2N} = S_{\text{plane}}^0 (1 + \frac{1}{N}), \quad (3.2)$$

so that in the large N limit on the sphere, the HF propagator approaches that on the flat plane.

Exactly the same diagrams appear in the free energy expansion for the spherical geometry as those for the plane. The contribution of each diagram with n vertices to the coefficient of the n th order term of the expansion is a product of a combinatorial factor and the integral/sum over the “momenta” along each line of the interactions at each vertex. The only differences on the sphere are these sums.

We now look at the lowest order Feynman graph without loops, shown in Fig. 1a, which has two vertices connected by four lines. The sum that appears in this diagram is $T^2 = \sum_{pqrs=0}^N \beta_{pqrs} \beta_{rspq}$. On the plane this is equal to $T_{\text{plane}}^2 = N/8$, and we find on the sphere:

$$T_{\text{sphere}}^2 = \frac{(N+1)^4}{4N^2(2N+1)} = \frac{N}{8} [1 + \frac{7}{2N} + \mathcal{O}(N^{-2})], \quad (3.3)$$

which also gives the result on the plane with a $1/N$ correction.

Generalizing our method to consider higher order terms, we calculate a particularly simple type of diagram to arbitrary order: the ring diagrams shown in Fig. 1b. For such a ring diagram of order n , the relevant sum

is $T^n = \sum_{p_i} \beta_{p_1 p_2 p_3 p_4} \beta_{p_3 p_4 p_5 p_6} \dots \beta_{p_{2n-1} p_{2n} p_1 p_2}$. We find on the sphere:

$$\begin{aligned} T_{\text{sphere}}^n &= \frac{(N+1)^{2n}}{2^n N^n (2N+1)^{n-1}} \\ &= T_{\text{plane}}^n [1 + \frac{3n+1}{2N} + \mathcal{O}(N^{-2})], \end{aligned} \quad (3.4)$$

where the result on a plane from Ref. 23 is $T_{\text{plane}}^n = 2^{1-2n} N$. So the contribution to the free energy to n th order approaches that on the plane as long as n is much less than the system size N . Although we have not verified this for more complex diagrams, we expect a similar result. This is because the interactions at each vertex have only $1/N$ (and higher power) corrections on the sphere from the interactions on the plane, so with n vertices in a diagram, there should be a total correction of order n/N . Therefore as long as the perturbation theory is useful (ie. on the high temperature side of any phase transition) the thermodynamic limit on the sphere should be the same as that for the flat plane. Intuitively, it is also reasonable that the free energy per vortex in the liquid phase should be the same on the flat plane and on the sphere. In the liquid phase, correlation lengths are finite (see Section V), and so long as they remain small compared to the sphere radius, then the liquid on the sphere is “unaware” of its curvature.

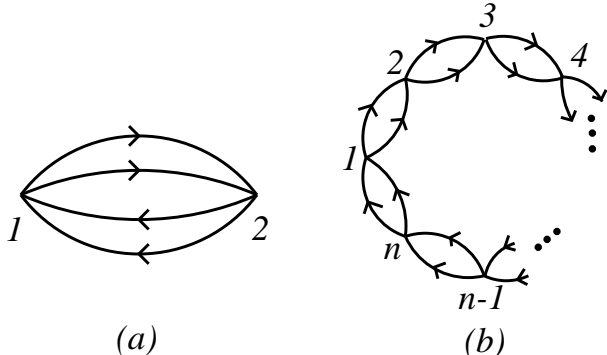


FIG. 1. Simple Feynman diagrams in the Free Energy series that we calculate on the spherical geometry: a) a second order diagram; b) part of the n th order ring diagram.

IV. GROUND STATES ON A SPHERE

The ground state of the LLL vortex system on an infinite plane was long ago discovered to be the triangular lattice.²⁴ This is also the ground state on the finite systems used in the QP simulations when commensurate boundary conditions are chosen. However, on a sphere the closest configuration the vortices can make to an ideal triangular lattice must contain twelve “disclinations”, i.e. twelve vortices that only have five nearest neighbors.

We have previously studied the ground states by numerical minimization of the Hamiltonian in Eq. (2.6) for different system sizes.¹⁷ The following conclusions were

made: there exist some values of N (magic numbers) for which the ground state has a lower energy than nearby values, and the energies as $N \rightarrow \infty$ do not seem to converge to the infinite plane value. Extrapolation of our numerical results gives an extra energy on the sphere in this large N limit of 0.2(4)% of the ground state energy per vortex on the infinite plane. The vortex configurations of these ground states make up a triangular network, but with twelve five-coordinated centers. The result that as $N \rightarrow \infty$ the ground states do not look the same as for an infinite plane may be explained by the presence of the disclinations (five-coordinated centers), which are defects with long range strains.²⁵ Therefore there will always be a finite fraction of the vortex system that is distorted from an ideal triangular lattice. This is supported by calculations within elasticity theory (which assumes only small distortions) that give a similar finite energy cost of the distortions on a sphere in the large N limit when an icosahedral arrangement of the disclinations is assumed.¹⁷

This result of an extra energy per vortex in the thermodynamic limit would be equally valid at finite temperatures as long as there is a non-zero shear modulus (ie. in a solid phase). If it were true there could be a paradox: Imagine a 2D system with a continuous phase transition from a liquid to a crystalline solid phase. Above the transition the free energies per vortex have been shown in Section III to be the same on the sphere and the plane and so this transition must remain at the same temperature in each case. As at the transition the free energy is continuous, then the free energies in the solid state must also be equal.

In fact, one can do a better job on the ground states on the sphere by having a number of dislocations (which are bound pairs of five-fold and seven-fold disclinations) in addition to the twelve free disclinations. This means we have to take away the restriction that every vortex is six-fold coordinated other than the twelve five-fold centers used in the elasticity calculation of Ref. 17. There is no topological problem with this as one can pull an opposite pair of dislocations out of a perfect lattice. That extra dislocation defects may lower the energy may be seen in two different ways. First, the interaction energy between a dislocation and a disclination may be negative, depending on the direction of the dislocation and this interaction energy grows faster with system size than the self energy of the dislocation. Alternatively, consider a region on a sphere bounded by three great circles that intersect at neighboring disclinations. Even in the large N limit this region will be distorted from a triangle (all three of its angles will be $2\pi/5$) and so a perfect triangular lattice in this region will be incommensurate with the boundaries, where a series of dislocations will occur. So we have a picture of a ground state in the large N limit made up of twenty regions of perfect lattice, but with sides containing dislocations, and corners containing disclinations.

There are still competing effects which discourage dislocations, and which may explain why they were not seen

in Ref. 17. First there is the curvature of the sphere which favors the distortions of a disclination, but which decreases as $1/R^2$. Second, there is the positive self energy of a dislocation, which is generally expected to increase as the logarithm of the system size.²⁶ Third there is the interaction between two dislocations which is directional, and approximately proportional to the logarithm of the distance between them. To estimate the density of dislocations needed to reduce the strain energy of the disclinations we use the framework of elasticity theory.

A. Elasticity calculation of defects on a sphere

The elasticity theory of twelve disclinations on a sphere is described in Ref. 17. The method is briefly explained here and then generalized to allow the inclusion of dislocations. We consider small strains from an ideal lattice, $u_{ij}(\mathbf{r})$. These strains are related to a stress field by Hooke's law, $\sigma_{ij} = 2\mu u_{ij} + \lambda u_{kk} \delta_{ij}$. For the LLL system the elastic constant λ diverges (the system is incompressible) and the shear modulus μ is given by $\mu = 0.48k_B T a_T^2 / 4\pi \beta_A^2 l_m^2$. The stress tensor has zero divergence which allows the problem to be expressed in terms of the Airy stress function, χ , defined by $\sigma_{ij} = \epsilon_{ik} \epsilon_{jl} \partial_k \partial_l \chi$. Five-fold disclinations are defined by the change in bond angle by $2\pi/6$ when a path encircles one such defect. Dislocations, on the other hand, are defined by their Burgers vector, but they are also equivalent to a disclination dipole pair. The stress field corresponding to a particular configuration of these topological defects is given by the solutions to the biharmonic equation on a sphere:

$$\frac{1}{K_0} \nabla^4 \chi = -\frac{1}{R^2} + \sum_{s=1}^{12} \frac{2\pi}{6} \delta(\mathbf{r} - \mathbf{r}_s) + \sum_d \epsilon_{ij} b_i^d \partial_j \delta(\mathbf{r} - \mathbf{r}_d), \quad (4.1)$$

where K_0 is the 2D Young's modulus which in the LLL system is given by $K_0 = 4\mu$. The free disclinations are labeled by s , and d labels the dislocations with Burgers vectors \mathbf{b}^d . In the large R limit where we neglect the energy of bending the lattice over the spherical curvature, the energy of a given configuration is

$$E_{el} = \frac{1}{2K_0} \int d^2 r (\nabla^2 \chi)^2 = \frac{1}{2K_0} \int d^2 r \sigma_{kk}^2, \quad (4.2)$$

where the integrals are over the surface of the sphere.

We will need to use coordinate frames rotated so that the reference axis passes through the defect. For instance, if a disclination is at the position (θ_s, ϕ_s) in our original coordinate frame, a general point (θ, ϕ) is described in the rotated frame by the coordinates $\theta'(s)$ (the polar angle from the disclination) and $\phi'(s)$ (the azimuthal angle in the rotated frame relative to the $\phi = \phi_s$ direction), where

$$\cos \theta'(s) = \cos \theta \cos \theta_s + \sin \theta \sin \theta_s \cos(\phi - \phi_s) \quad (4.3)$$

$$\sin \theta'(s) \sin \phi'(s) = \sin \theta \sin(\phi - \phi_s) \quad (4.4)$$

$$\sin \theta'(s) \cos \phi'(s) = \sin \theta \cos \theta_s \cos(\phi - \phi_s) - \cos \theta \sin \theta_s. \quad (4.5)$$

For the reference direction of the azimuthal angle $\phi'(s)$ in the new frame also to be rotated, a further transformation $\phi'(s) \rightarrow \phi''(s)$ is required (as in the standard treatment of Euler angles²⁷). We use this extra rotation for the dislocation defects, but for simplicity we do not define the transformation here.

The solution of Eq. (4.1) in the absence of dislocations was found to be $\chi = \sum_{s=1}^{12} \chi_s$ where the s th disclination is at (θ_s, ϕ_s) and

$$\nabla^2 \chi_s(\theta, \phi) = \sigma_{kk}^s(\theta, \phi) = \frac{K_0}{12} \left\{ \ln \frac{1}{2} [1 - \cos \theta'(s)] + 1 \right\}. \quad (4.6)$$

The elastic energy cost of the twelve disclinations is $E_{12} = R^2 \int d\Omega [\sum_s \sigma_{kk}^s(\theta, \phi)]^2$, which is proportional to the area of the system, and gives a finite energy cost per vortex.

If we now consider additional dislocation defects, we may write $\chi = \sum_s \chi_s + \sum_d \chi_d$ where

$$\frac{1}{K_0} \nabla^4 \chi_d = \epsilon_{ij} b_i^d \partial_j \delta(\mathbf{r} - \mathbf{r}_d). \quad (4.7)$$

By differentiating the solution for a disclination, we find:

$$\sigma_{kk}^d(\theta, \phi) = \frac{K_0 l_0}{4\pi R} \frac{\sin \theta'(d) \sin \phi''(d)}{1 - \cos \theta'(d)}, \quad (4.8)$$

where we take the size of the Burgers vector to be the lattice spacing l_0 , and $\phi''(d)$ is the azimuthal angle about the axis through the dislocation measured from the direction of the Burgers vector.

Within elasticity theory, we can consider separately the contributions of the self energy of each defect, and the pairwise interaction energy between the defects. The self energy of a dislocation on a sphere is

$$E_d = -\frac{K_0 l_0^2}{32\pi} \left\{ 1 + \cos(a/R) + 2 \ln \frac{1}{2} [1 - \cos(a/R)] \right\} + E_{core}, \quad (4.9)$$

where a is a cutoff of the order of the lattice spacing (within a of the dislocation, the linear elasticity theory must break down completely) and E_{core} is the energy of the distortion inside this cutoff. As expected, this becomes proportional to $\ln(R/a)$ in the limit of large R , where:

$$\lim_{R \rightarrow \infty} (E_d) = \frac{K_0 l_0^2}{16\pi} [2 \ln(R/a) + 2 \ln 2 - 1] + E_{core}. \quad (4.10)$$

In the presence of more than one dislocation the total elastic energy will be

$$E_{tot} = \frac{1}{2K_0} \int d^2r \left(\sum_{s=1}^{12} \sigma_{kk}^s + \sum_{d=1}^{N_d} \sigma_{kk}^d \right)^2 \quad (4.11)$$

$$= E_{12} + N_d E_d + \sum_{s=1}^{12} \sum_{d=1}^{N_d} E_{sd}(\mathbf{r}_s, \mathbf{r}_d, \mathbf{b}^d) \\ + \sum_{d=1}^{N_d} \sum_{d'>d}^{N_d} E_{dd}(\mathbf{r}_d, \mathbf{r}_{d'}, \mathbf{b}^d, \mathbf{b}^{d'}), \quad (4.12)$$

which is a sum of the self energies plus pairwise interactions between every defect (the interactions between disclinations are included in E_{12}).

If we consider a disclination at $(\theta_s, \phi_s) = (0, 0)$ and a dislocation at (θ_d, ϕ_d) with a Burgers vector pointing perpendicular to the $\phi = \phi_d$ line (such that the five-seven pair in the dislocation point towards the disclination), we find an interaction energy:

$$E_{sd}(\mathbf{r}_s, \mathbf{r}_d, \mathbf{b}^d) = -\frac{K_0 l_0 R}{12} \left[\frac{(1 - \cos \theta_d)}{\sin \theta_d} \ln \frac{1}{2} [1 - \cos(\theta_d)] \right]. \quad (4.13)$$

Allowing the dislocation to rotate by an angle γ will give the above energy multiplied by a factor $\cos \gamma$.

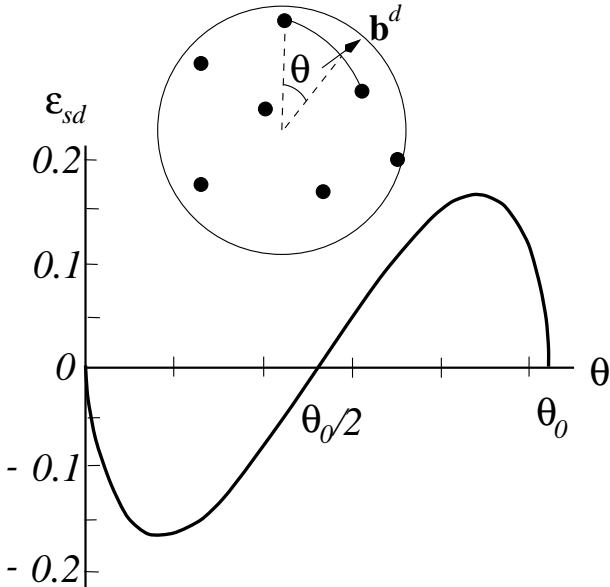


FIG. 2. The interaction energy $E_{sd}^{icos} = (K_0 l_0 R / 12) \epsilon_{sd}$ between a dislocation and twelve disclinations in an icosahedral configuration, where the dislocation is on a line between two neighboring disclinations, with a Burgers vector perpendicular to the line. The polar angle θ_0 between two neighboring disclinations is defined in the text. The polar angle between the dislocation and the disclination is θ as shown in the diagram, where the spots represent the positions of disclinations on the sphere.

The interaction energy between two dislocations, one at $(\theta_{d'}, \phi_{d'}) = (0, 0)$, the other at (θ_d, ϕ_d) , with opposite Burgers vectors perpendicular to the line joining the dislocations, is found to be

$$E_{dd}(\mathbf{r}_{d'}, \mathbf{r}_d, \mathbf{b}^{d'}, \mathbf{b}^d) = \frac{K_0 l_0^2}{4\pi} \left[1 + \frac{\ln \frac{1}{2} [1 - \cos \theta_d]}{(1 + \cos \theta_d)} \right]. \quad (4.14)$$

Again as expected, the total energy of a dislocation pair, $2E_d + E_{dd}$, in the large R limit becomes proportional to the logarithm of the distance between the two opposite dislocations.

Notice that the interaction energy between a dislocation and disclination increases more rapidly with R than the self energy and the dislocation-dislocation interaction energy. As E_{sd} may be negative (depending on the orientation of the Burgers vector), there is an instability to the formation of dislocations, for large enough system size. If we consider the twelve disclinations to be fixed at the corners of an icosahedron, we find the energy landscape of a single dislocation to have minima along the lines that join the disclinations. The energy E_{sd}^{icos} (which is a sum of the interactions between the dislocation and the twelve disclinations) is shown in Fig. 2 as a function of position on one of these lines, with a Burgers vector that is perpendicular to the line. The position is denoted by the polar angle θ from one disclination, with a neighboring disclination located at $\theta = \theta_0 = 2 \tan^{-1}[(\sqrt{5} - 1)/2]$. By symmetry, the energy is zero exactly on a disclination and at the midpoint between two disclinations, and there is one negative stationary point.

For an estimate of when dislocations should first start to appear in the ground states as R increases, we consider the energy to put two dislocations of opposite Burgers vectors on each line joining disclinations, at the positions that minimize E_{sd} . Such a configuration has an elastic energy cost of

$$E_{tot} = E_{12} + K_0 l_0^2 [-0.861(R/l_0) + 2.39 \ln(R/l_0) + 0.907] \\ + 60E_{core}, \quad (4.15)$$

where we assume $a = l_0$ and have only taken into account the dislocation-dislocation interactions between pairs on the same line. If we neglect E_{core} we find that $E_{tot} = E_{12}$ when $R = 6.05l_0$ which corresponds to $N \simeq 530$. However, with an estimate of $E_{core} \sim K_0 l_0^2 / 16\pi$, this critical value increases to $N \simeq 1000$. The critical value of N is sensitive to the estimated values of the core energy, and the neglect of extra dislocation pair interactions. Also, we have neglected the local curvature, which for small systems will favor the presence of the disclination strains, and therefore disfavor dislocations that screen these strains. Our estimates are compared with numerical results later in this section.

Having established that dislocations may lower the total elastic energy cost on the sphere for large enough

systems, it remains to show that large numbers of dislocations may screen out the strain field of the disclinations so as to cancel the R^2 dependence of the elastic energy.

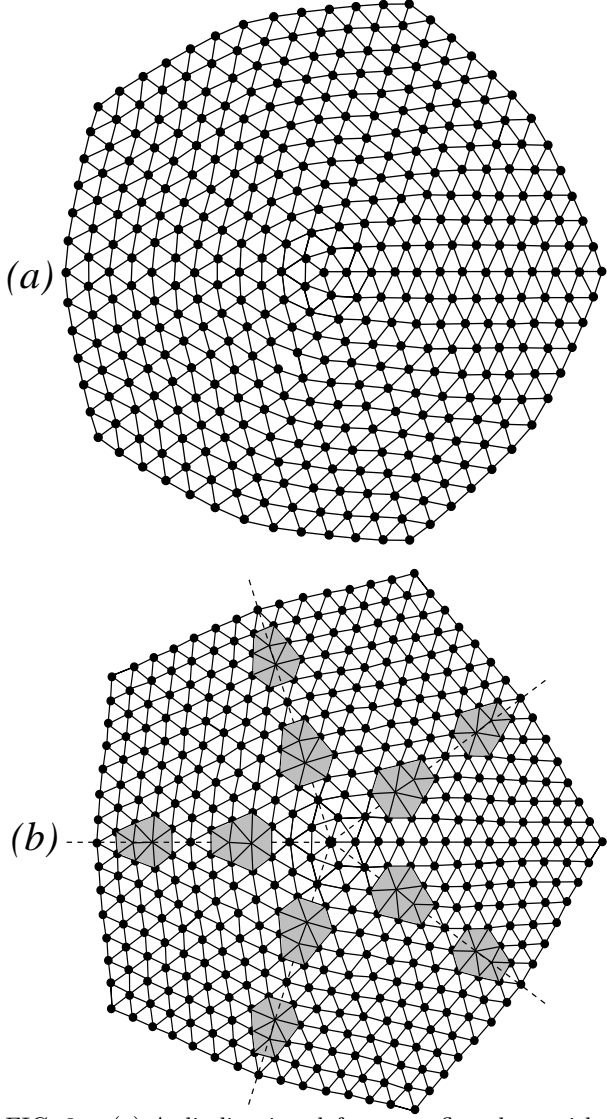


FIG. 3. (a) A disclination defect on a flat plane without dislocations. (b) An example of dislocation series screening a disclination on a flat plane.

We consider series of dislocations along the lines between the disclinations. The sum of the strains from each defect may be approximated at large distances by an integral. For such a series with equally spaced dislocations a distance cl_0 apart, the resulting strain fields are those from a positive and a negative disclination at each end of the line, but with a charge of size $q_s = 1/c$ (where $q_s = +1$ for a five-fold disclination). This charge arises from the ratio of the distance between the five-seven pair in a dislocation to the distance between dislocations in the series. This is seen by writing the sum of the dislocation strain fields as an integral. A series of dislocations

running from $(0, 0)$ to some point $(\Theta, 0)$ will have a total strain field of

$$\begin{aligned}\sigma^c(\theta, \phi) &\simeq \frac{R}{cl_0} \int_0^\Theta \sigma_{\theta'}^d(\theta, \phi) d\theta' \\ &= \frac{1}{c} \sigma_\Theta^s(\theta, \phi) - \frac{1}{c} \sigma_0^s(\theta, \phi),\end{aligned}\quad (4.16)$$

because the strain field $\sigma_{\theta'}^d(\theta, \phi)$ of a dislocation at $(\theta', 0)$ with Burgers vector perpendicular to the $\phi = 0$ direction is just the differential of the strain field $\sigma_{\theta'}^s(\theta, \phi)$ of a disclination: $\sigma_{\theta'}^d = l_0 [\partial \sigma_{\theta'}^s / \partial (R\theta')]$.

If we imagine such series with $c = 5$ between each disclination and the midpoints to neighboring disclinations, as is shown near one disclination in Fig. 3, then the strain field of each disclination will be exactly screened away. However, there will be an effective disclination of charge $q_s = 2/5$ at each midpoint [the midpoint makes a polar angle $\theta_m = \theta_0/2$ with the disclination, so that $\tan \theta_m = (\sqrt{5} - 1)/2$]. What is needed is a variable spacing that starts from $5l_0$ at the disclination, but diverges at the midpoint. We may require that the spacing has the scaling form $c(\theta') = 5 + (R/l_0)g(\theta')$ with the condition that $g(0) = 0$ (this form is chosen as any higher power of R would lead to a spacing that increases faster than the length of the series).

In the large N limit an exact cancellation of the R^2 terms in the energy is obtained. The strain field from one series starting at $\theta = 0$ and lying along $\phi = 0$ is given by

$$\begin{aligned}\sigma^c(\theta, \phi) &= \int_0^{\theta_m} \sigma_{\theta'}^d(\theta, \phi) c^{-1}(\theta') R d\theta' \\ &= [\sigma_{\theta'}^s(\theta, \phi) c^{-1}(\theta')]_0^{\theta_m} - \frac{l_0}{R} \int_0^{\theta_m} \sigma_{\theta'}^s(\theta, \phi) \frac{dg^{-1}}{d\theta'} d\theta' \\ &= -\frac{1}{5} \sigma_0^s + \frac{1}{[5 + (R/l_0)g(\theta_m)]} \sigma_{\theta_m}^s - \frac{l_0}{R} I(\theta, \phi),\end{aligned}\quad (4.17)$$

where $I(\theta, \phi) = \int_0^{\theta_m} (dg^{-1}/d\theta') \sigma_{\theta'}^s d\theta'$, which remains of order one as the system size increases. In the large R limit we write the strain field of the i th series that is connected to the disclination j as $\sigma_{i,j}^c(\theta, \phi) = -(1/5) \sigma_j^s(\theta, \phi) + g^{-1}(\theta_m) (l_0/R) \sigma_{i,j,\theta_m}^s(\theta, \phi) - (l_0/R) I_{i,j}(\theta, \phi) \equiv -(1/5) \sigma_j^s + (l_0/R) f_{i,j}$ where i runs from one to five. The elastic energy cost due to all the defects, $E_{tot} = E_{12} + E_{sd} + E_{dd}$ is

$$\begin{aligned}E_{12} &= \frac{R^2}{2K_0} \int d\Omega \sum_{j,j'=1}^{12} \sigma_j^s(\theta, \phi) \sigma_{j'}^s(\theta, \phi) \\ &\equiv \frac{1}{2K_0} \sum_{j,j'=1}^{12} R^2 \epsilon_{jj'} \\ E_{sd} &= -\frac{1}{K_0} \left(\sum_{j,j'=1}^{12} R^2 \epsilon_{jj'} - l_0 R \sum_{j,j'=1}^{12} \sum_{i=1}^5 \int d\Omega \sigma_{j'}^s f_{i,j} \right)\end{aligned}$$

$$\begin{aligned}
E_{dd} &= \frac{1}{2K_0} \sum_{j,j'=1}^{12} \left(R^2 \epsilon_{jj'} + 2l_0 R \sum_{i=1}^5 \int d\Omega \sigma_{j'}^s f_{i,j} \right. \\
&\quad \left. + 2l_0^2 \sum_{i,i'=1}^5 \int d\Omega f_{i,j} f_{i',j'} \right) \\
E_{tot} &= \frac{l_0^2}{K_0} \sum_{j,j'=1}^{12} \sum_{i,i'=1}^5 \int d\Omega f_{i,j}(\theta, \phi) f_{i',j'}(\theta, \phi), \quad (4.18)
\end{aligned}$$

which shows that all of the terms of order R^2 cancel, leaving terms of order one which depend on the gradients of $g^{-1}(\theta')$ and the value of $g^{-1}(\theta_m)$. Our approximation in simplifying the effective charge at the midpoint to be proportional to $1/R$ ignores a correction of order $1/R^2$ to this charge. As the energy of a disclination is proportional to the area of the system, the energy cost of this ignored extra charge is also of order one. Therefore, the production of these series of dislocations of variable spacing, along the lines between disclinations, is an effective way of screening the diverging strains of the disclinations. The ground state energy per vortex in the large N limit is the same as that for an infinite flat plane apart from a correction proportional to $N^{-1/2}$ due to the core energies of the dislocations.

B. Numerical evidence for dislocations in ground states

We now consider the numerical evidence for the above conclusions. It is sufficient to minimize the Hamiltonian of Eq. (2.6) by minimizing the Abrikosov ratio

$$\beta_A = \frac{\langle |\psi|^4 \rangle}{\langle |\psi|^2 \rangle^2} = \frac{\sum_{p=0}^{2N} |U_p|^2}{\left(\sum_{q=0}^N |U_q|^2 \right)^2}. \quad (4.19)$$

The triangular lattice on the flat plane has the value²⁴ $\beta_{A,0} \simeq 1.1596$. In Ref. 17, the ground states of system sizes up to $N = 652$ were found numerically, and it was suggested that there was a finite energy cost per vortex in the large N limit, consistent with the presence of twelve disclinations. The existence of magic numbers was observed and explained, although for large systems this only has a small effect on the total energy.

We have extended this investigation to larger systems; this is motivated by the above elasticity results which suggest that above a critical size, dislocations will appear in the ground states and these will screen the strains of the disclinations to recover the large N limit ground state energy of the flat plane. In Fig. 3 the sort of configuration is shown that we expect to find near each disclination. This figure demonstrates just how large the spherical system must be to accomodate the dislocations and screen out the strains over a large region.

In Fig. 4 our numerical results are shown for ground states of systems larger than $N = 652$ up to $N = 2432$.

We also include results from Ref. 17 for smaller system sizes. It is important to note that, as the systems get large, there is an increasing number of metastable states that the minimization routines may fall into. In each case we have taken the lowest energy after several hundred runs, but this is always just an upper bound on the true ground state energy.

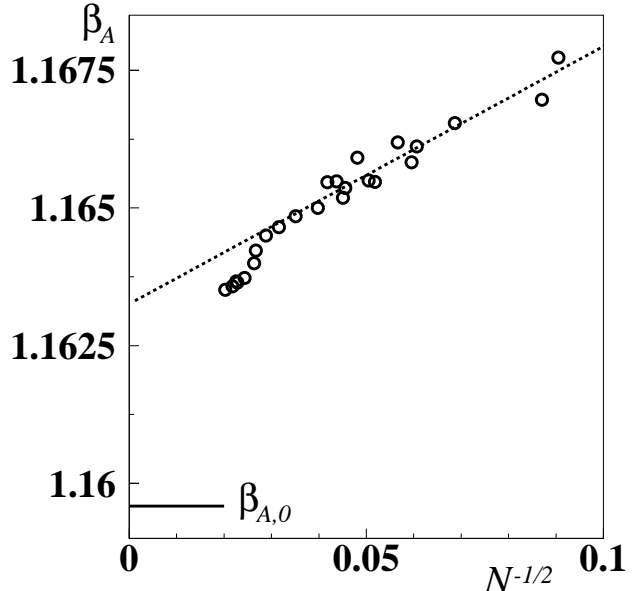


FIG. 4. The Abrikosov ratio of numerically found ground states for different system sizes. Only magic number systems are shown. The straight line fit to $N^{-1/2}$ is only on data for $N < 1400$. Above this value, dislocations are seen in the ground states and β_A falls under the fit.

Plotting the Abrikosov ratio against $N^{-1/2}$ the results for $N < 1200$ fall on a straight line that extrapolates to give a finite difference for the flat plane as $N \rightarrow \infty$. However, this trend changes above $N = 1200$, with energies falling below the straight line. The results are explained by the reasoning that once systems are large enough for dislocations to overcome their self energy and mutual repulsion, they may screen the strains of the disclinations and reduce the total ground state energy. In the numerical ground states with $N > 1200$ we observe dislocations near the disclinations with the correct orientation of Burgers vector (the distribution of the dislocations may be irregular due to the difficulties in locating the true global ground state).

The elasticity calculation combined with this numerical work is strong evidence that the ground state energy per vortex in the thermodynamic limit is the same on the sphere as on the flat plane. It should be mentioned however that for the system sizes we look at in MC simulations, the ground states have a higher energy per vortex by 0.5-1% of the ground state energy on an infinite plane. The jump in the energy at the transition observed in the

QP systems is of a similar order of magnitude ($\sim 1\%$) as the energy difference of the spherical ground states from the QP ground states. It must be a possibility that the raising of the ground state energy inhibits a freezing transition to the low temperature state, which could explain the apparent absence of a phase transition in our simulations on the sphere.

V. SIMULATIONS ON THE SPHERE

We now go on to measure the correlations in the 2D vortex system using MC simulations. In the following, the system sizes we often use correspond to the magic numbers with particularly low energy ground states. This is because a phase transition would be most likely where the ground state is least frustrated. Also, where we start the simulations in the ground state, we have most confidence that our numerical ground states are the correct ones in the magic number cases. However, we fail to observe commensurability effects in the MC simulations. The magic numbers are a property of the ground state, and do not affect the vortex liquid over the temperature range investigated.

A. The Density Correlation Function

O'Neill and Moore have investigated the correlation function associated with vortex positions.⁷ This method is unwieldy as it requires finding the roots of an N th order polynomial at every measurement. It is more convenient to look at the four point density correlation function (briefly investigated by Lee and Moore¹⁹ and related to the correlator studied on the QP systems¹²)

$$\chi(\mathbf{r} - \mathbf{r}') = \langle |\psi(\mathbf{r})|^2 |\psi(\mathbf{r}')|^2 \rangle - \langle |\psi(\mathbf{r})|^2 \rangle \langle |\psi(\mathbf{r}')|^2 \rangle. \quad (5.1)$$

This is most revealing in reciprocal space. On a spherical surface this means that we need to decompose the function into spherical harmonics:

$$\chi_l^m = \int d\Omega d\Omega' \chi(\mathbf{r} - \mathbf{r}') Y_l^{m*}(\theta, \phi) Y_l^m(\theta', \phi'). \quad (5.2)$$

Within the LLL subspace, this correlator can be written as thermal averages over the coefficients u_p :

$$\begin{aligned} \chi_l^m = & \frac{\pi N^2 \bar{\rho}^2}{\left(\sum_{p=0}^N \langle u_p^* u_p \rangle \right)^2} \left[\sum_{p,q,r,s=0}^N I_{p,q,l}^m I_{r,s,l}^m \langle u_p^* u_q u_r^* u_s \rangle \right. \\ & \left. - \frac{\delta_{l,0}}{\pi N^2} \left(\sum_{p=0}^N \langle u_p^* u_p \rangle \right)^2 \right], \quad (5.3) \end{aligned}$$

with $I_{p,q,l}^m$ given in Appendix B and $\bar{\rho}$ equal to the mean density $\bar{\rho} = \langle |\psi|^2 \rangle$. To make comparison with different

temperatures we look at the function $C_l^m = \chi_l^m / \bar{\rho}^2$ and then normalize this function by its infinite temperature limit $C_{l,\infty}$ (also given in Appendix B). We average our measurements over m , so our investigations center on the function $\Delta(k) = \sum_{m=-l}^l C_l^m / [(2l+1)C_{l,\infty}]$ with $k = l/R$. $\Delta(k)$ is the same correlator that has been looked at in a plane geometry by Hu and MacDonald¹² as well as by Yeo and Moore,²⁸ but modified for a sphere. Examples of this function for different α_T and N are shown in Fig. 5.

We have concentrated our measurements on the form of the peak in $\Delta(k)$ at the first reciprocal lattice vector. In our units for a triangular lattice with a unit cell of area ϕ_0/B this is given by $|\mathbf{G}| \simeq 2.694$. In the entire temperature range we look at ($\alpha_T \geq -12$) we find that a Lorentzian always gives an excellent fit to this peak (see Fig. 5). This is consistent with an exponential decrease of the density correlations in real space. The associated correlation length ξ_D is easily extracted from the width δ of the peak at half its maximum, as $\xi_D \propto 1/\delta$. In Fig. 6 we plot $1/\delta$ against α_T for different system sizes, which shows how the correlation length grows as the temperature is lowered, and reveals when finite-size effects become important. Down to $\alpha_T = -10$ the results for the larger systems appear to be independent of system size. For $\alpha_T < -8$, finite size effects for $N = 132$ make its values of δ^{-1} fall beneath the trend of the larger systems. A linear fit at low temperatures is at least consistent with the results from vortex-vortex correlations⁷ that $\xi_D \sim |\alpha_T|$, as $|\alpha_T| \rightarrow \infty$.

For small $|\alpha_T|$ corrections to this scaling form are apparent, so that the range of this fit is small. Nevertheless, it is clear that there is no jump in the value of ξ_D in the vicinity of the observed transition of QP simulations, or the predicted KTHNY transition. For the integral of $\Delta(k)$ under a given peak to remain constant we would expect the general form $\Delta(k) \sim \xi_D f(\xi_D(k - G))$ in the vicinity of the peak.²⁸ This implies that the peak height is proportional to the inverse width. Using the parameters from our Lorentzian fits, this relation is demonstrated in the inset of Fig. 5.

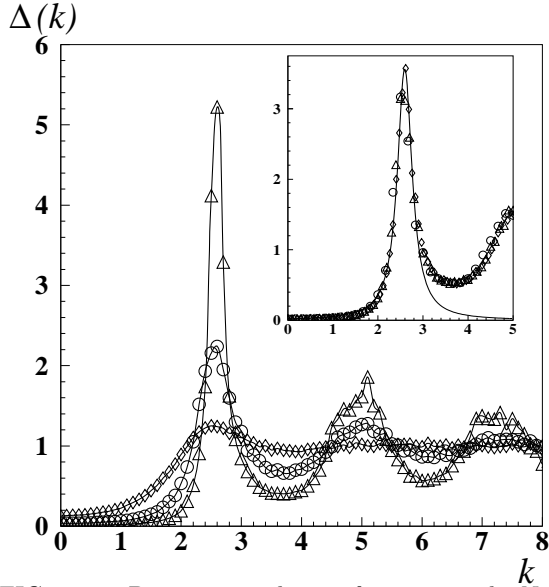


FIG. 5. Density correlation function with $N = 200$ for reduced temperatures $\alpha_T = -2, -5$ and -10 (the peak heights increase with lower temperatures). The inset shows the density correlation function at $\alpha_T = -8$ with $N = 72, 200$ and 400 . The solid line is a Lorentzian fit when $N = 400$.

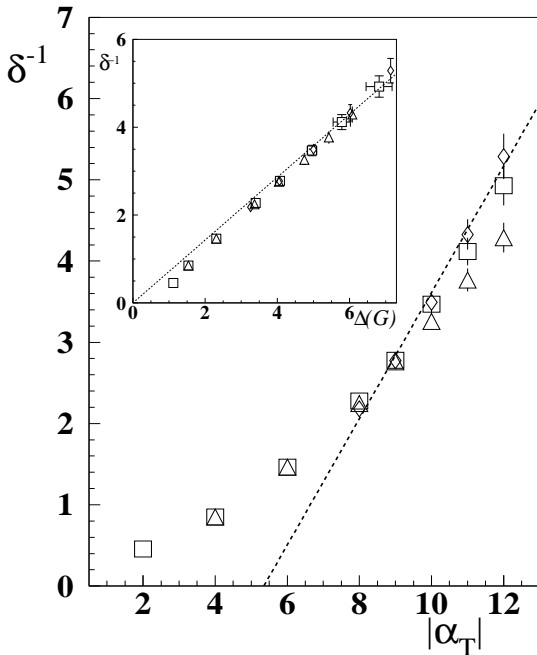


FIG. 6. Inverse width of the first peak in $\Delta(k)$ with temperature. The inset shows the inverse width against the peak height at different temperatures. The triangles, squares and diamonds represent $N = 132, 192$ and 402 respectively. The straight line is a fit to the $N = 402$ points for $|\alpha_T| \geq 8$.

These results should be compared to those of Yeo and Moore where $\Delta(k)$ was calculated within a high temperature approximation that uses a non-perturbative method to go to lower temperatures.²⁸ In this work similar zero temperature scaling is seen down to $\alpha_T = -10$, although the peak heights do not grow as fast.

In contrast, Hu and MacDonald,¹² who calculate $\Delta(k)$ with an MC simulation on a plane with periodic boundary conditions, see an order of magnitude jump in the peaks at a transition temperature of $\alpha_T \sim -9$. Below this first order transition, $\Delta(k)$ shows “Bragg peaks” at the reciprocal lattice vectors. However, in the temperature range above this freezing, the correlation function appears to be quantitatively the same as on the sphere at the same temperature. This is as it should be as the liquid phase on the sphere has the same properties as the liquid on the flat plane as long as the system size is sufficiently large.

B. Real Space Phase Correlations

It is long range coherence in the phase of the order parameter (ODLRO) that gives rise to superconductivity. Within the LLL approximation the phase can only be changed by the movement of the vortices, so one might expect a simple relation between vortex correlations and phase coherence. Sasik, Stroud and Tesanovic¹⁴ have defined a phase correlation function as $\sigma(\mathbf{r} - \mathbf{r}') = \langle \psi^*(\mathbf{r})\psi(\mathbf{r}') \rangle / \bar{\rho}$. From measurements of this in their MC simulation with QP boundary conditions they found that in the thermodynamic limit $\sigma(r)$ fell to zero over the order of a lattice constant even when in the solid phase characterized by long range density correlations.

As our model is always in the liquid state it is clear that $\sigma(r)$ will always be trivially short ranged simply due to the translations of the vortex system. However we are interested in the phase correlations between points moving in the same patch of correlated vortices. It is the length scale associated with this type of correlation that is physically relevant. That is, when this length scale approaches the limiting scale of a given sample (eg. the distance between pinning centers) it will become superconducting. To investigate this length scale we need to measure the correlations in the phase from a fixed vortex. We also need to fix the rotations about this vortex (these would also destroy phase coherence). In practise we can do this by (a) fixing one vortex at a pole ($\theta = 0$) by setting $u_0 = 0$, and (b) fixing the nearest six vortices by keeping $u_i = u_i^{(0)}$ for $i = 1, 2, \dots, 6$. $\{u_i^{(0)}\}$ are the coefficients for the ground state with a fixed orientation. These conditions effectively fix the order parameter in a local region around the central fixed vortex. We can then measure the correlation between the phase at a point $\mathbf{r}' = (\theta', \phi')$ and at $\mathbf{r} = (0, 0)$:

$$\sigma_{fix}(\mathbf{r}') = \langle \psi^*(\mathbf{0})\psi(\mathbf{r}') / |\psi^*(\mathbf{0})||\psi(\mathbf{r}')| \rangle_{fix}. \quad (5.4)$$

Note the difference between this and the correlation function of SST. As well as the fixing of the vortices, our definition contains no part dependent on the amplitude of the order parameter. In terms of the MC variables, the phase at $\theta = 0$ is given by $\psi(0, \phi)/|\psi(0, \phi)| = u_1 e^{i\phi}/|u_1|$ where ϕ is the azimuthal angle of approach as $\theta \rightarrow 0$. Fixing this angle ϕ to be zero, the phase correlation function may be written as

$$\sigma_{fix}(\theta', \phi') = \left\langle \frac{u_1^* \sum_{m=1}^N u_m h_m \sin^m(\theta'/2) \cos^{N-m}(\theta'/2) e^{im\phi'}}{\left| u_1^* \sum_{m=1}^N u_m h_m \sin^m(\theta'/2) \cos^{N-m}(\theta'/2) e^{im\phi'} \right|} \right\rangle_{fix}. \quad (5.5)$$

FIG. 7. The top diagrams show the phase correlation function $|\sigma_{fix}(\theta, \phi)|$ plotted in the complex z -plane where $z = \tan(\theta/2)e^{i\phi}$ for $\alpha_T = -6, -9$ and -11 , with $N = 72$. The bottom row shows the mean density $\langle |\psi(\mathbf{r})|^2 \rangle_{fix}/\bar{\rho}$ with the same fixed coefficients as for the phase correlations. Notice that one of the fixed vortices is a five-fold center.

without apparently encircling any vortex results in a phase change of $2N\pi$ (this is the origin of the Dirac quantization of the charge on a monopole). This does not imply a singularity in the supercurrent, as the gauge part of the current will exactly cancel with this wave function contribution.

Our measurements of $\sigma_{fix}(\theta, \phi)$ are shown in Fig. 7 using the projection $z = \tan(\theta/2)e^{i\phi}$. For comparison, we also show the mean density $\langle |\psi(\mathbf{r})|^2 \rangle_{fix}$ with the same coefficients fixed. A growing range of phase coherence as the temperature is lowered is demonstrated, and coincides with the growth in density correlations. The length scale ξ_{phase} is found by plotting σ_{fix} against $R\theta$ and fitting a gaussian over the region outside the fixed vortices, i.e. for $R\theta > a$ with $a = 2.5$. We find that ξ_{phase} increases proportionally to $|\alpha_T|$ in the temperature range $\alpha_T < -7$ (see Fig. 8), with again corrections to scaling visible for $\alpha_T \gtrsim -7$. The similarity between Figures 6 and 8 indicates that the length scales for phase and density coherence grow proportionally to each other as the temperature is reduced. The length scales are unchanged within the measured errors for the different system sizes studied. A relation between the growth of correlations in the density $|\psi|^2$ and in the phase of ψ is clearly observed.

The scaling of phase coherence $\xi_{phase} \sim |\alpha_T|l_m$ was predicted by O'Neill and Moore from two distinct arguments. One of these involved considering the thermal excitation of small amplitude shear modes from the ground state lattice to define a phase coherence length within the crystalline phase. The second argument considered the free energy cost of phase fluctuations over a finite region of the vortex system. It is this second argument that is directly relevant to the liquid phase with a finite length scale of crystalline order, and we repeat and amplify it here. The free energy cost of phase fluctuations over a region with crystalline correlations was shown to be $F_{eff} = (d/2) \int d^2r c_{66} l_m^4 (\nabla_\perp^2 \Phi)^2$, where Φ is the phase

The reader may notice a problem in measuring the phase of a complex function on the surface of a sphere. If a path is followed that encircles one vortex, the phase of ψ will change by 2π . However, an ambiguity exists in the definition of the inside or the outside of a closed loop in a closed surface and this could lead to an ill defined phase. In fact, it is our choice of gauge that places on one axis a string (or infinitely long and thin solenoid) terminating at the monopole that removes this ambiguity. This choice effectively makes the South pole ($\theta = \pi$) the “outside” of the system, and the North pole ($\theta = 0$) the center. This results in a singularity in the phase of the order parameter at $\theta = \pi$. Encircling the South pole

of the order parameter. From this result, the free energy cost of a phase change of π over a region of linear extent ξ will be $F(\xi) \sim c_{66} d l_m^4 \xi^{-2}$. When such excitations proliferate, phase coherence will be destroyed. Hence, there will be phase coherence only over the length scale ξ when the free energy $F(\xi)$ is of order $k_B T$. The α_T dependence of the mean-field elastic shear modulus c_{66} is known in the large field limit, $c_{66} \simeq \alpha_T^2 k_B T / d l_m^2$, with the simple result that $\xi \sim |\alpha_T| l_m$.

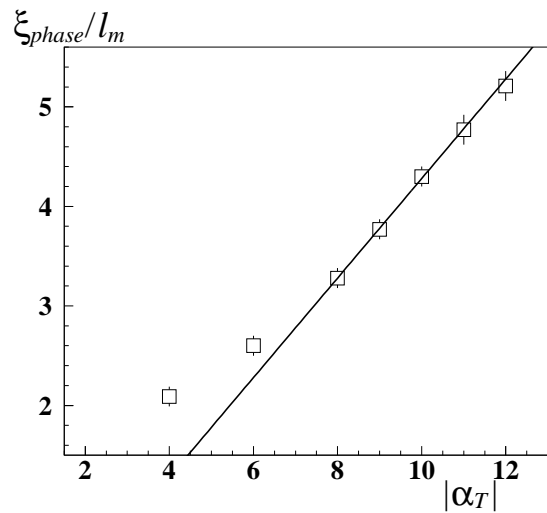


FIG. 8. The length scale associated with phase coherence extracted from $\sigma_{fix}(\theta, \phi)$ with $N = 192$ against temperature.

We believe that there is another kind of phase fluctuation within the liquid that can be identified with a topological defect— a “braid”. Consider a ring of vortices of a given radius that move around the circumference of

the ring. (In three dimensions this vortex movement may take place along the field direction to form a topologically constrained defect—hence the name, braid. We have previously calculated the energies of such defects.²⁹⁾ Such a movement may be created by a simple combination of changes to the basis coefficients. If we make the transformation $u_m \rightarrow u'_m = u_m e^{i\gamma}$ for $m = 0, 1, 2, \dots, \nu$ and make no change to the remaining coefficients $m = \nu + 1, \dots, N$ then such a braid movement will occur in a ring of vortices that enclose approximately ν vortices (see Fig. 9).

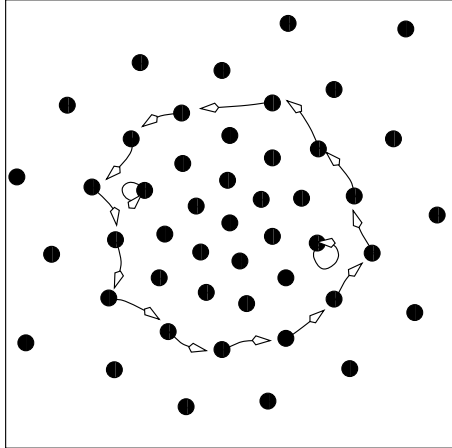


FIG. 9. The path of vortices under the change $u_m \rightarrow u'_m = u_m e^{i\gamma}$ for $m = 0, 1, 2, \dots, \nu$ as γ goes from 0 to 2π with $\nu = 20$. In this case the original state is the ground state for $N = 72$. The vortices are plotted in the complex z -plane where $z = \tan(\theta/2)e^{i\phi}$.

If $\gamma = 2\pi$ the vortices in the ring will each hop to a neighbors position, with a phase change in the order parameter of 2π inside the ring (i.e. no essential change). Excitations will involve values of γ less than 2π which increase the phase at the center of the ring by γ while leaving the phase unchanged outside of the ring. The energies of these braid excitations will define a length scale over which they proliferate, and thus destroy phase coherence. The energy costs of braids in a crystal phase would increase with the size of the ring, and so phase coherence would not be destroyed by this mechanism in the crystalline state. Nevertheless, we believe that the excitations of such defects are present on the length scale ξ in the liquid phase, and are a plausible mechanism for the loss of phase coherence seen in Fig. 7. Notice that in Fig. 7 it is when the density correlations become ring-like (as would happen due to braid excitations) that the phase coherence is lost.

VI. EFFECT OF AN INHOMOGENEOUS MAGNETIC FIELD

If an experiment using the spherical geometry was ever to be realized, there would always be a problem in plac-

ing the end of a solenoid (the “monopole”) exactly at the center of the sphere. This will cause the external field to be inhomogeneous over the surface of the sphere. Such inhomogeneities are generic in experiments with any geometry, so it is worthwhile investigating these effects.

We consider displacing the monopole from the center of the sphere by a distance d along the z -axis. It is straightforward to show that for small $\epsilon = d/R$, this induces a change in the vector potential of $\delta \mathbf{A} = \epsilon B_0 R \sin \theta \hat{\phi}$. An inhomogeneity is introduced into the magnetic field at the surface which has a radial component of $B_r = B_0(1 + 2\epsilon \cos \theta)$. Substituting this new field into the free energy gives an extra term to first order in ϵ of

$$\delta F = \frac{\tilde{\epsilon}}{N} \sum_{m=0}^N |v_m|^2 (2m - N), \quad (6.1)$$

where $\tilde{\epsilon} = (d\hbar^2 Q^2/2m)\epsilon$.

Before we look at our MC results with this extra term, we consider its effect within the high-temperature perturbation theory. With the addition of (6.1) to the Hamiltonian, the HF equation becomes

$$\tilde{g}_m = g_m (1 - 2\tilde{g}_m \sum_p \tilde{g}_p \beta_{pmpm}), \quad (6.2)$$

with $g_m = \alpha_T + \tilde{\epsilon}(2m - N)/N$. The sum in this equation is no longer independent of m . However, in the large N limit, β_{pmpm} has the form,

$$\lim_{N \rightarrow \infty} (\beta_{pmpm}) = \frac{1}{2\Delta\sqrt{\pi}} \exp[-(p - q)^2/\Delta^2], \quad (6.3)$$

where $\Delta = [(2N - p - q)(p + q)/4N]^{1/2}$. The width of the interaction is of order $N^{1/2}$ over most of the sphere. If the variation in the renormalized propagator \tilde{g}_p is smooth over the range of $N^{1/2}$ (which corresponds to changes in real space being smooth over the distance l_m) then the sum over p is dominated by contributions when $p \simeq m$ to give $\sum_p \tilde{g}_p \beta_{pmpm} \simeq \tilde{g}_m/2$. Therefore we have $N + 1$ independent HF equations $\tilde{g}_m = g_m (1 - \tilde{g}_m^2)$. Each has the same solution, but with an m -dependent effective temperature: $\tilde{g}_m = (\alpha_m/2)[-1 \pm (1 + 4/\alpha_m^2)^{1/2}]$ with $\alpha_m = \alpha_T + \tilde{\epsilon}(2m - N)/N$. This will be true for any change in the Hamiltonian of the form $\delta F = \sum_{m=0}^N \epsilon(m) |v_m|^2$. where the effective temperature becomes $\alpha_m = \alpha_T + \epsilon(m)$. Such a change corresponds to changes in real space in one direction only over length scales longer than l_m .

This procedure can be generalized to an arbitrary diagram in the perturbative scheme. Any diagram is dominated by contributions where the indices in and out of a vertex are within Δ of each other. Therefore a given diagram is just the sum of the respective diagrams without the inhomogeneity but at the effective temperature α_m . For example, the free energy may be expanded in a power series of the propagator, $F_{\text{pure}}(\alpha_T) = N \sum_{n=0}^{\infty} a_n \tilde{g}^{2n}$. With the inhomogeneity this generalizes to

$$F_{inhom}(\alpha_T, \tilde{\epsilon}) = \sum_{n=0}^{\infty} \sum_{p=0}^N a_n \tilde{g}_p^{2n} = \frac{1}{N+1} \sum_{p=0}^N F_{pure}(\alpha_p). \quad (6.4)$$

This result may break down when variation in $\epsilon(m)$ is on a scale less than $N^{1/2}$. In the thermodynamic limit our conclusion will hold as long as the perturbation expansion remains useful.

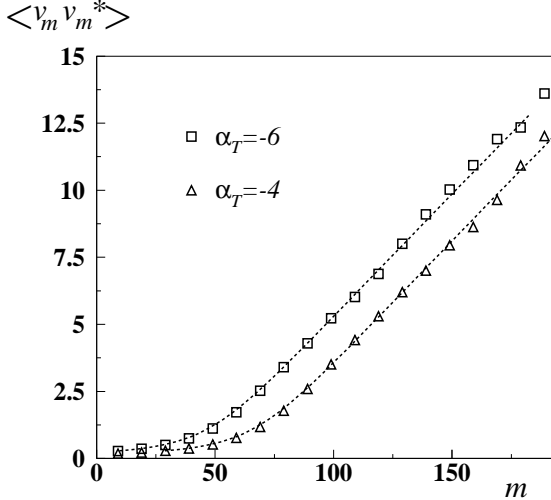


FIG. 10. The m dependent propagator for two different strengths of inhomogeneity with $N = 192$ and $\tilde{\epsilon} = -10$. The dashed line represents the value of the propagator in the pure case at the effective temperature $\alpha_T = \alpha_m$. Note that the effective temperature covers the range $-16 < \alpha_m < +4$.

Interesting effects may occur when there is a phase transition in the pure system. However, as our simulations fail to see such a transition, the above analysis is sufficient to explain our numerical results. In Fig. 10 we plot the m -dependent propagator $|v_m|^2$ from MC simulations with $\tilde{\epsilon} = -10$, and compare to the zero inhomogeneity propagator with the m -dependent effective temperature. The results confirm that the system behaves with the local properties of the effective temperature.

VII. DISCUSSION OF SIMULATIONS WITH DIFFERENT GEOMETRIES

In this section we discuss some of the problems of different boundary conditions when interpreting the results of numerical simulations of superconducting thin films within the LLL approximation. We first mention some of the shortcomings of the spherical geometry used in our simulations. We then go on to discuss the other main geometry used—QP boundary conditions. In this case there exist problems not present in the spherical geometry due to the constraints on the phase of the order parameter.

We also consider a third geometry with a circular geometry, where initial work has not found a phase transition. Finally, we look at the implications of recent experiments.

A. The spherical geometry

An important difficulty on the sphere is that the crystalline state free energy is raised due to the curvature and the necessary presence of twelve disclinations. A liquid with correlation length less than the system size will be unaffected by the curvature. The energy difference should disappear in the thermodynamic limit (see Section IV). However, for the system sizes studied, this energy remains on the same order of magnitude of the jump in energy seen at the transition observed with QP boundary conditions.

The presence of the topologically required disclinations on the sphere is clearly an important feature not present in real thin films. However, their effects will only become important as the correlation length of the system approaches the distance between disclinations. This is a finite size effect as experienced by any geometry, although the effective system size will be smaller for a given N than on a plane. For the largest system sizes studied, finite-size effects probably become important in the region of interest at $\alpha_T \sim -10$.

The mobility of these disclinations, if large, would be a mechanism for destroying crystalline order in a finite-sized system. At low temperatures the disclinations should not be mobile, both because of their mutual repulsion (as can be seen from the elasticity calculation) and the topological barrier to their motion through the lattice. At higher temperatures where there is a finite density of dislocations (eg. in a hexatic phase) the dislocations provide a topological mechanism for the motion of the disclinations. In finite size systems, the strain field associated with the disclination may even create dislocations by pulling apart the dislocation pairs that are always present in a 2D crystal. From inspection of snapshots of the systems at finite temperatures we have observed that dislocations are attracted to the disclinations, and that the positions of the disclinations are not perfectly icosahedral as they are in the ground states.

Our measurements so far have been insensitive to hexatic bond-angle order. This order could never be globally defined on the sphere, and will only be a meaningful concept within the regions free of any disclinations, which are small in the system sizes we study.

It must be conceded, therefore, that our numerical evidence from the sphere for the non-existence of a phase-transition is not yet conclusive. Larger system size studies are clearly needed, but even increasing sizes by an order of magnitude may not resolve the problem. Our work on the ground states suggests that very large systems with $N \sim 10^4$ may be needed to reach certain properties of the thermodynamic limit such as the screening

of the disclinations by dislocations.

B. Quasi-periodic boundary conditions

In the system investigated by Refs. 10–14 a constant magnetic field \mathbf{H} perpendicular to a thin-film superconductor is represented by the Landau gauge, $\mathbf{A} = -By\hat{x}$. In this gauge the LLL states are $\psi_p(x, y) = \exp[ipk_0x - (y - pk_0l_m^2)/2l_m^2]$, where k_0 is a “momentum” in the x direction that must be fixed by the boundary conditions. For a general state in the LLL subspace, $\psi(x, y) = Q \sum_p c_p \psi_p(x, y)$, the system is periodic in the x direction with period $L_x = 2\pi/k_0$. Quasi-periodicity in the y -direction may also be imposed by setting $c_{m+N} = c_m$. This condition leads to $\psi(x, y + L_y) = \exp(iNk_0x)\psi(x, y)$ with $L_y = Nk_0l_m^2$. So each principle region has an area $L_x L_y = 2\pi N l_m^2$ and contains N zeros of ψ that correspond to vortices. To have a geometry commensurate with a triangular vortex lattice, $N_x = L_x/l_0$ and $N_y = L_y/(\sqrt{3}l_0/2)$ are fixed as integers. (Note the difference between the magnetic length l_m and the lattice spacing l_0 both of which are defined in Section II.)

The difference between this system and more conventional periodic boundary conditions comes from the constraints on the phase of the order parameter as the principal region is crossed. That such a constraint exists is apparent from the fact that there are only $2N$ degrees of freedom available to describe the $2N$ coordinates of the vortex positions as well as an overall phase and amplitude. It has been shown that the phase constraints lead to the center of mass of the vortex positions to be fixed,³⁰ which accounts for the missing two parameters. A consequence of the fixed center of mass is that there are only N distinct ground states, each a triangular lattice separated by a minimum discrete distance.

In MC simulations with QP boundary conditions, evidence is seen for a first order transition. The observed melting temperature drops as system size is increased but extrapolation gives an estimate for the thermodynamic transition¹² at $\alpha_T = -9.3 \pm 0.1$. In the low temperature state dominated by the ground state there is a finite energy barrier between different ground states. We now estimate what that energy barrier is.

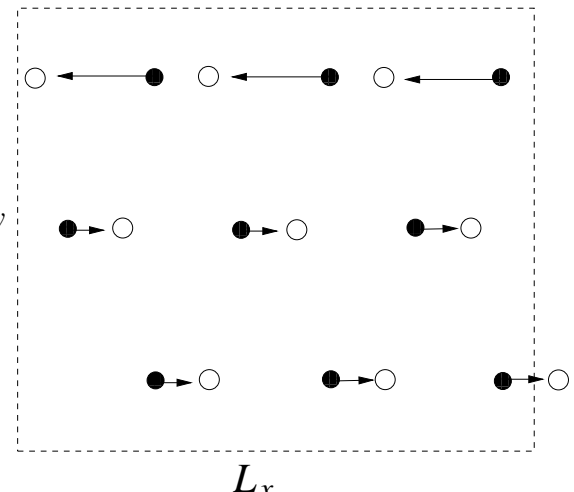


FIG. 11. Two possible ground states for $N = 9$ with QP boundary conditions. A path between the two ground states is shown that leaves the position of the center of mass unchanged. Note that only the principal region is shown.

Figure 11 illustrates the sort of movement of vortices between ground states that obeys the center of mass constraint. The example is for $N = 9$, and a short inspection will reveal that there are only 9 distinct ground states that may be related by such moves. In general the different ground states have the form $c_{p-q_1} = \exp[i(\pi/2)(p/N_x)^2 - 2i\pi(p + N_x q_1)q_2/N]$ for p equal to an integer multiple of N_x , and zero otherwise. Each ground state is labeled by ψ_{q_1, q_2} , where q_1 must be an integer from 1 to N_x , and the condition $c_p = c_{p+N}$ quantizes the allowed values of q_2 to integers from 1 to N_y . These ground states are exactly equivalent to the Eilenberger³¹ states $\phi(\mathbf{r}|\mathbf{r}_0)$, with $\mathbf{r}_0 = (x_0, y_0)$ where $x_0 = q_2 l_0/N_y$ and $y_0 = q_1(\sqrt{3}/2)l_0/N_x$. These are related by $\phi(\mathbf{r}|\mathbf{r}_0) = \exp[2\pi i(2y_0/\sqrt{3})x]\phi(\mathbf{r} + \mathbf{r}_0|\mathbf{0})$.

Consider the change $c_p \rightarrow c'_p = c_p e^{ip\gamma}$ for any configuration of $\{c_p\}$. For an infinite system this just corresponds to a uniform translation of the vortices in the x direction by γ/k_0 . However, with QP boundary conditions this change will involve movement of vortices at the edges of the principal region in the opposite direction, thus conserving the center of mass. (An analogous change in the spherical geometry gives the braid in Section V B.) It is exactly this sort of movement that is a path between different ground states. For example, if we start from $\psi_{0,0}$ and apply this transformation with γ changing from 0 to $2\pi q_2/N$ we arrive at the state ψ_{0,q_2} .

What is the energy barrier for such a path? The free energy of the QP system is given by

$$\mathcal{H}(\{c_m\}) = k_B T \alpha_T^2 \left[\operatorname{sgn}(\alpha_T) \sum_{m=0}^{N-1} |c_m|^2 + \frac{1}{2N_x} \sum_{p=0}^{N-1} \sum_{q,r,s=-\infty}^{\infty} \beta_{pqrs} c_p c_q c_r^* c_s^* \right], \quad (7.1)$$

with $\beta_{pqrs} = 3^{1/4} 2^{-1/2} \delta_{p+q,r+s} e^{\{-(p-q)^2 + (r-s)^2\} \sqrt{3}\pi/4N_x^2}$. Changing the phase of the coefficients does not affect the quadratic energy. Also, the contributions to the quartic term $\beta_{pqrs} c_p c_q c_r^* c_s^*$ will be zero when p, q, r , and s correspond to the same region (ie. they are all between 0 and $N - 1$). As the width of the gaussian in the quartic interaction is of order N_x , contributions will be negligible unless these variables are within $\sim N_x$ of each other, and the edge of the principal region. Therefore the energy barrier of this path will be of order $N^{1/2}$. This N dependence has been observed numerically.³²

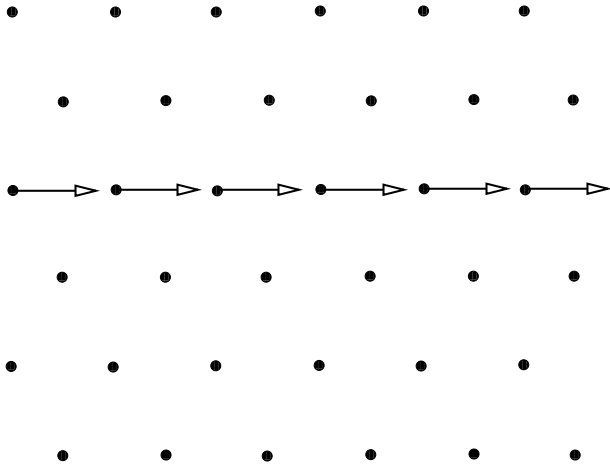


FIG. 12. The relative motion of vortices when moving between two neighboring ground states in the QP system.

A more quantitative estimate may be obtained by considering the movement of the vortices at the edge of the principal region relative to the vortices in the bulk of this region (see Fig 12). At any point on the path this represents a defect from the perfect ground state, the energy cost of which may be calculated using the methods of Ref. 29. We find an energy barrier of

$$E_b = 0.33(L_x/l_0)\alpha_T^2, \quad (7.2)$$

which is proportional to N_x as predicted. This is an upper bound, as only the movement of a line of vortices has been allowed, without relaxation of the surrounding lattice. However, as the interaction energy is short ranged,²⁹ we do not expect the N dependence to change. It is also a zero temperature result, but it should still hold for a low temperature state with long correlations. We emphasize that this energy barrier grows with system size, despite the fact that the positions of the discrete ground states get closer to each other.

Additional evidence for the size of these barriers comes from the simulations themselves. In Ref. 14 a plot is shown of $\langle |\psi(\mathbf{r})|^2 \rangle$ at a temperature corresponding to the extrapolated thermodynamic transition, where the modulations in this quantity show that the system is dominated by just one of the N ground states during the length of the measurement, 10^6 MC steps.

The measurements by SST of this low temperature state are clearly not equilibrated as not all of the ground states are being sampled; there should always be a translationally invariant density for any *finite* system. It is also a possibility that energy barriers between ground states affect the evidence for a first order phase transition. For instance, the free energy of the liquid will be overestimated if the simulation is not run for long enough (the standard time for these simulations has been $\sim 10^6$ MC steps) which may alter the melting temperature. This casts doubt on the extrapolation of the melting temperature to the thermodynamic limit. Even if a first order (or continuous) transition remains after full equilibration, the discrete ground state problem makes the QP system unsuitable for transport measurements.

C. The circular geometry on a flat plane

An alternative set of boundary conditions may be constructed in the symmetric gauge,⁷ $\mathbf{A} = (x\hat{\mathbf{y}} - y\hat{\mathbf{x}})B/2$. The LLL states may be formed by the complete basis with circular symmetry $\psi_m = \zeta^m \exp[-|\zeta|^2/(4l_m^2)]$, where $\zeta = x + iy$. To perform numerical simulations, one has to truncate the series of these states to a finite number of terms, say, $m = 0$ to N . This truncated system has N vortices, as $\psi = \sum_{m=0}^N c_m \psi_m = \exp[-|\zeta|^2/(4l_m^2)] \prod_{i=1}^N (\zeta - \zeta_i)$, and the order parameter drops rapidly to zero outside of a radius $(2N)^{1/2}l_m$ from the origin.

Little work has been done on this geometry as finite size effects are strong. Numerical minimizations on small systems have shown that the ground state energy per vortex is *lower* than for the infinite plane,³³ and vortices near the edge of the system are attracted to the “boundary”³² (near where the order parameter is zero). The finite size effects are greater than with spherical or QP boundary conditions where there are no edges of the finite systems and each vortex resides in an equivalent local environment. The effect of the boundary is mainly in a fraction of $\sim N^{-1/2}$ of the bulk of the system, and should be unimportant in the thermodynamic limit.

A similar geometry has been used in simulations of the 2D one component plasma (OCP), where the particles are confined to a circular disk.³⁴ A first order transition was observed and this contrasts with the absence of a transition in simulations of the OCP on a spherical geometry.³⁵ This has motivated us to perform simulations on the circular geometry in search of a phase transition. We have performed the real space phase and density correlation measurements as in Section VB for systems up to $N = 400$ and find results consistent with those on the sphere. We have also measured the internal energy while heating from the ground state and cooling from high temperatures, for system sizes up to $N = 1000$. These energy measurements (see Fig 13) have revealed no

hysteresis on the scale observed in the QP system for temperatures greater than $\alpha_T = -12$, and hence no evidence for a phase transition.

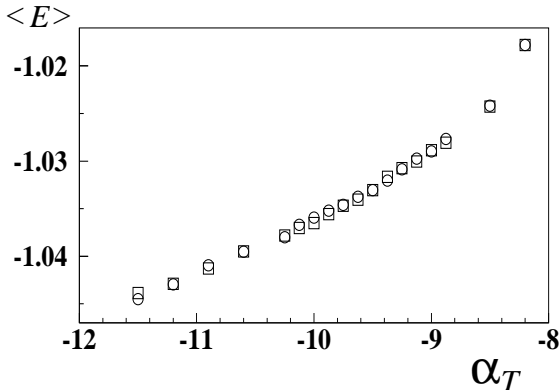


FIG. 13. The mean internal energy from MC measurements on the circular geometry with $N = 1000$. The circles represent measurements while the temperature is being raised; the squares represent cooling. Each measurement is averaged over 30 000 MC steps. The energy is normalized by the ground state energy per vortex on the infinite plane.

D. Experiments

It seems that from a theoretical point of view there are three possible scenarios for the behavior of thin film superconductors in the presence of a magnetic field: a) the standard picture of KTHNY melting of a 2D crystal where a dislocation mediated continuous transition occurs between a low temperature state with quasi-crystalline order and a high temperature liquid or hexatic phase; b) a first order transition where the liquid free energy becomes lower than the solid phase before KTHNY melting takes place (as is seen in QP simulations); c) the absence of a distinct low-temperature state, but where the correlation lengths of the liquid diverge as $T \rightarrow 0$ (this is the prediction of high order perturbation theory from the high temperature side, and is consistent with the numerical simulations on the sphere). We now discuss some experimental results and their implications for these possibilities.

A melting transition of the flux lattice in $\text{In}/\text{In}0_x$ thin films was observed by Gammel *et al.*² The zero field limit of the transition was consistent with the Kosterlitz-Thouless transition in the absence of external fields, though the magnetic field dependence of the melting line did not satisfy the predictions of the KTHNY theory. The measured transitions were mainly at low fields, so the relevance of our simulations here are doubtful.

In the experiments of Berghuis *et al.*³ the current voltage response was measured of amorphous $\text{Nb}_{1-x}\text{Ge}_x$ films at different fields and temperatures. A drop to zero in the a.c. ohmic resistivity is seen, for example at fields

$H \sim 0.8H_{c2}$ at $T = 0.68T_c$, though the d.c. response remains finite (ie. the critical current is zero.). This drop is attributed to a KTHNY transition consistent with the temperature and film thickness dependence of the melting field. A similar conclusion is made by Yazdani *et al.*⁴ from a.c. measurements on films of amorphous $\text{Mo}_{77}\text{Ge}_{23}$.

It should be emphasized that these a.c. measurements at a given frequency ω probe structural changes of the vortex system over a restricted length scale.⁴ While this is useful to measure properties independent of the presence of a large pinning length, one would expect even in the absence of a phase transition to see a large drop in the resistivity at fixed frequency when the relaxation times grow larger than $1/\omega$. In numerical simulations on the sphere,¹⁹ the plastic time scale was observed to increase as $\tau_{pl} \sim \exp(A\alpha_T^3)$ and we would expect a sharp drop when $\tau_{pl} \sim 1/\omega$.

In contrast to the above experiments, measurements by Nikulov *et al.*⁵ on films of amorphous NbO_x with weak pinning have found no signatures of a resistive transition down to fields $\sim 10^{-3}H_{c2}$. This implies that the transitions observed previously are not universal properties of superconducting thin films. While the lack of a resistive drop may be attributed to the total absence of pinning, one would expect in the presence of a first order transition, where there is a discontinuous change in $\langle|\psi|^2\rangle$, that this would be observed as a step in the flux flow resistivity.

Thus the interpretation of these experiments remains controversial. While the KTHNY theory provides a useful framework to discuss flux lattice melting in two dimensions, its effects have only been observed over short length scales.⁴ As far as we know there has been no experimental indication of a first order transition in superconducting thin films. In principle, the results of these experiments can still be explained simply by the growing length scales and relaxation times of a vortex liquid in the absence of a phase transition.

VIII. CONCLUSIONS

We have shown that the model with a spherical geometry remains in the vortex liquid phase, at least down to temperatures $\alpha_T \gtrsim -12$ for system sizes up to $N \leq 402$. This could be due to the raised energy of the ground states because of the necessary presence of twelve disclinations in a triangular network over a sphere. However, we have made similar investigations on an alternative finite size model: considering the LLL basis states on an infinite plane with a circular symmetric gauge and truncating the series to include only N vortices.⁷ This system has a lower ground state energy per vortex than the infinite system and no disclinations, but we see the same length scales as in Section V B for temperatures down to $\alpha_T = -12$. The main evidence for a first order transition

in the QP model is the double peak structure observed in the probability distribution of the internal energy at the transition. Our investigations on the internal energy for both the sphere and the plane with circular coordinates have revealed no such signatures.

The fact that the spherical system remains in the liquid phase down to low temperatures allows us to measure the variation of the correlations in the liquid state with temperature over a large regime. Measurements in the liquid phase have the advantages that the system reaches equilibrium over a reasonable time scale at low temperatures. Our measurements of the density correlations are consistent with those in the liquid phase using QP boundary conditions.¹² The extracted length scales demonstrate an asymptotic linear dependence on $|\alpha_T|$. The scaling analysis of O'Neill and Moore predicted that the *phase coherence* length should grow as $\xi_{\text{phase}} \sim |\alpha_T|$. Our results for the phase coherence are consistent with this scaling form, and also demonstrate that in the liquid the phase and density correlations grow with identical temperature dependence.

Our results for the scaling of the phase correlations contradict the conclusions of SST, who claim that in the thermodynamic limit $N \rightarrow \infty$ the phase coherence has a range only of the order of the lattice spacing in their “solid” phase. However, this discrepancy is really due to different definitions of what is meant by phase coherence. SST do not predict the growth of the length scale of phase correlations as the temperature goes to zero. Although their results are claimed as evidence for the charge-density wave of Tesanovic,¹⁶ a finite length scale that grows with decreasing temperature or even a power law form of ODLRO would still be consistent with this exotic phase. It seems unlikely to us that the low-temperature phase below a first order transition would have a shorter range of phase coherence than the liquid phase. If we measure the phase correlations without fixing any vortices, we also find no phase coherence beyond a length of one lattice spacing, due to the translational freedom of the liquid phase. In the solid phase of the QP model the vortex system appears to be fixed near one ground state due to the finite energy barrier between the N ground states, and this allows phase coherence to be observed over a long range. As N increases, there is a decrease in the range of phase coherence. These measurements by SST demonstrate just how strong the finite-size effects are in the QP simulations below the observed transition. Without fixing the motion of any vortices, the phase coherence should always have a trivial length scale of the inter-vortex spacing. By restricting the motion of a small number of vortices, we have been able to measure a more physically relevant phase correlation length that is consistent with the expected growth of order as the temperature is reduced. An interesting question remains as to whether a similarly defined phase coherence in the solid phase with QP boundary conditions would result in true long range order, or another length scale that also exhibits zero temperature scaling.

Despite the differences in results from spherical and QP boundary conditions, our results from high temperature perturbation theory and on the ground states suggest that the thermodynamic limit will be the same on the sphere as the infinite flat plane. This contradicts the earlier statement of Ref. 17 where the effect of allowing additional dislocation defects into the ground state was not considered. Even so, the results on the ground states show how large system sizes must be for certain properties to approach the thermodynamic limit. A definite drawback on the sphere is the small effective system size compared to the number of degrees of freedom.

The spherical geometry is perhaps not only relevant for simulational purposes. It is possible that an experiment could be constructed with an amorphous type-II superconductor sputtered over the surface of a sphere, and one end of a long and thin solenoid inserted into the center to approximate the field from a monopole. In contrast an experimental realization of the QP boundary conditions is not possible (these boundary conditions are primarily of interest in extrapolating to the thermodynamic limit of an infinite number of free vortices). We feel that the spherical geometry, with its property of translational invariance, remains a useful system for numerical simulations, especially to measure properties of the unpinned vortex liquid. An investigation into dynamical properties with a view to examining the length scales associated with non-local resistivity³⁶ is planned, which would not be possible using QP boundary conditions due to the absence of full translational invariance of the vortex positions.

ACKNOWLEDGMENTS

We would like to acknowledge useful interactions with Gianni Blatter, Tom Blum, Vadim Geshkenbein, Roman Sasik and Joonhyun Yeo. MJWD would also like to thank Han Lee for the use of his source code and the EPSRC for financial support.

APPENDIX A: DEPENDENCE OF THE HAMILTONIAN ON VORTEX POSITIONS

In this appendix we will show that the GL free energy Hamiltonian in Eq. (2.6) depends only on the positions of the zeros in the order parameter on the sphere. First, from Eq. (2.7) we have

$$\begin{aligned} \psi(\theta, \phi) &= C \prod_{i=1}^N [\sin(\theta/2)e^{i\phi} - z_i \cos(\theta/2)] \\ &= D \prod_{i=1}^N [a_i \sin(\theta/2)e^{i\phi} - b_i \cos(\theta/2)] \end{aligned}$$

$$= D \prod_{i=1}^N f_i(\theta, \phi), \quad (\text{A1})$$

with $D = C \prod_{i=1}^N z_i/b_i$ and $b_i = a_i z_i$. If $f_i = 0$ when $\theta = \theta_i$ and $\phi = \phi_i$ then we may choose:

$$\begin{aligned} a_i &= \cos(\theta_i/2) e^{-i\phi_i/2} \\ b_i &= \sin(\theta_i/2) e^{i\phi_i/2}. \end{aligned} \quad (\text{A2})$$

Now, the GL-LLL free energy is a functional that depends only on the value of $|\psi|^2 = |D|^2 |\prod_{i=1}^N f_i|^2$ at each point on the sphere. If we can show that $|f_i(\theta, \phi)|^2$ depends only on the relative position of the i th zero then the Hamiltonian will be invariant with respect to coordinate rotations of all the zeros:

$$\begin{aligned} |f_i(\theta, \phi)|^2 &= \left| \cos(\theta_i/2) \sin(\theta/2) e^{i(\phi-\phi_i)/2} \right. \\ &\quad \left. - \sin(\theta_i/2) \cos(\theta/2) e^{-i(\phi-\phi_i)/2} \right|^2 \\ &= \frac{1}{2} [1 - \cos(\theta) \cos(\theta_i) - \sin(\theta) \sin(\theta_i) \cos(\phi - \phi_i)] \\ &= \frac{1}{2} [1 - \cos \theta'(i)] \\ &= \sin^2[\theta'(i)/2] \end{aligned} \quad (\text{A3})$$

where $\theta'(i)$ is the polar angle measured from the axis through the i th zero to the point (θ, ϕ) , defined by an analogous expression to Eq. 4.3. This is independent of the coordinate frame and so we have shown that $|\psi(\theta, \phi)|^2$ depends only on the relative positions of the vortices plus the overall amplitude.

APPENDIX B: DETAILS FOR DENSITY CORRELATIONS

To find the reciprocal space density correlator from thermal averages of the LLL basis state coefficients (see Eq. (5.3)) we need the integrals

$$I_{p,q,l}^m = h_p h_q \int_0^\pi \int_0^{2\pi} d\theta d\phi e^{i(q-p)\phi} \sin \theta \sin^{p+q}(\theta/2) \times \cos^{2N-p-q}(\theta/2) Y_l^m(\theta, \phi), \quad (\text{B1})$$

which may be written:

$$\begin{aligned} I_{p,q,l}^m &= \delta_{p-m,q} (-1)^m h_p h_{p-m} \left[\frac{(2l+1)(l+m)!}{4\pi(l-m)!} \right]^{1/2} \times \\ &\quad \times \frac{4\pi p!(N-p+m)!}{(N+m+1)!m!} {}_3F_2 \left[\begin{matrix} m-l, m+l+1, p+1 \\ m+1, N+m+2 \end{matrix} \right], \end{aligned} \quad (\text{B2})$$

where ${}_3F_2[a, b, c; d, e]$ is a generalized hypergeometric series. To find the infinite temperature limit of C_l^m we consider the case $m = 0$ and calculate the averages $\langle v_p v_q^* v_r v_s^* \rangle$ and $\langle v_p v_q^* \rangle$ exactly in the limit $\alpha_T \rightarrow +\infty$ (this involves only Gaussian integrals). Our result is

$$\begin{aligned} C_{l,\infty} &= \frac{(2l+1)}{(N+1)^2} \sum_{p=0}^N {}_3F_2 \left[\begin{matrix} -l, l+1, p+1 \\ 1, N+2 \end{matrix} \right]^2 \\ &= \frac{(N!)^2}{(N-l)!(N+l+1)!}. \end{aligned} \quad (\text{B3})$$

(We are indebted to T. Blum for this final result.) This is consistent with the fact that in the limit $N \rightarrow \infty$, the infinite temperature correlation function should be identical with that for an infinite plane,¹² and the expression in Eq. (B3) should tend to $\exp(-l^2/N)$.

¹ D. S. Fisher, Phys. Rev. B **22**, 1190 (1980); B. A. Huberman and S. Doniach, Phys. Rev. Lett. **43**, 950 (1979).

² P. L. Gammel, A. F. Hebard and D. J. Bishop, Phys. Rev. Lett., **60**, 144 (1988).

³ P. Berghuis and P. H. Kes, Phys. Rev. B **47**, 262 (1993); P. Berghuis, A. L. F. van der Slot and P. H. Kes, Phys. Rev. Lett. **65**, 2583 (1990).

⁴ A. Yazdani, W. R. White, M. R. Hahn, M. Gabay, M. R. Beasley and A. Kapitulnik, Phys. Rev. Lett. **70**, 505 (1993).

⁵ A. V. Nikulov, D. Y. Remisov and V. A. Oboznov, Phys. Rev. Lett. **75**, 2586 (1995).

⁶ M. A. Moore, Phys. Rev. B **39**, 136 (1989); **45**, 7336 (1992).

⁷ J. A. O'Neill and M. A. Moore, Phys. Rev. Lett. **69**, 2582 (1992); Phys. Rev. B **48**, 374 (1993).

⁸ P. A. M. Dirac, Proc. R. Soc. London, Ser. A **133**, 60 (1931).

⁹ J. Pearl, Appl. Phys. Lett. **5**, 65 (1964).

¹⁰ Z. Tesanovic and L. Xing, Phys. Rev. Lett. **67**, 22729 (1991); L. Xing and Z. Tesanovic, Physica C **196**, 241 (1992).

¹¹ Y. Kato and N. Nagaosa, Phys. Rev. B **47**, 2932 (1993); **48**, 7383 (1993).

¹² J. Hu and A. H. MacDonald, Phys. Rev. Lett. **71**, 432 (1993); Phys. Rev. B **49**, 15263 (1994).

¹³ R. Sasik and D. Stroud, Phys. Rev. B **49**, 16074 (1993).

¹⁴ R. Sasik, D. Stroud and Z. Tesanovic, Phys. Rev. B **51**, 3042 (1995).

¹⁵ D. R. Nelson, in *Phase Transitions and Critical Phenomena*, edited by C. Domb and J. L. Lebowitz (Academic Press, New York, 1983), Vol. 7, p. 5.

¹⁶ Z. Tesanovic, *Physica C* **220**, 303 (1994).

¹⁷ M. J. W. Dodgson, *J. Phys. A: Math. Gen.* **29**, 2499 (1996).

¹⁸ S. M. Roy and V. Singh, *Phys. Rev. Lett.* **51**, 2069 (1983).

¹⁹ H. H. Lee and M. A. Moore, *Phys. Rev. B* **49**, 9240 (1994).

²⁰ N. Metropolis, A. W. Rosenbluth, M. N. Rosenbluth, A. H. Teller and E. Teller, *J. Chem. Phys.* **21**, 1087 (1953).

²¹ G. J. Ruggeri and D. J. Thouless, *J. Phys. F: Metal Phys.*, **6**, 2063 (1976).

²² J. Hu, A. H. MacDonald and B. D. McKay, *Phys. Rev. B* **49**, 15263 (1994); E. Brezin, A. Fujita and A. Hikami, *Phys. Rev. Lett.* **65**, 1949 (1990).

²³ G. P. McCauley and D. J. Thouless, *J. Phys. F: Metal Phys.*, **6**, 109 (1976).

²⁴ W. H. Kleiner, L. M. Roth and S. H. Autler, *Phys. Rev.* **133**, 1226 (1964).

²⁵ H. S. Seung and D. R. Nelson, *Phys. Rev. A* **38**, 1005 (1988).

²⁶ F. R. N. Nabarro, *Theory of Crystal Dislocations* (Clarendon Press, Oxford, 1967), pp. 53-7.

²⁷ H. Goldstein, *Classical Mechanics* (Addison-Wesley, 1980), pp. 143-8.

²⁸ J. Yeo and M. A. Moore, *Phys. Rev. Lett.* **76**, 1142 (1996).

²⁹ M. J. W. Dodgson and M. A. Moore, *Phys. Rev. B* **51**, 11887 (1995).

³⁰ F. D. M. Haldane and E. H. Rezayi, *Phys. Rev. B* **31**, 2529 (1985).

³¹ G. Eilenberger, *Phys. Rev.* **164**, 628 (1967).

³² R. Sasik (private communications).

³³ J. A. O'Neill, PhD thesis (University of Manchester).

³⁴ Ph. Choquard and J. Clerouin, *Phys. Rev. Lett.* **50**, 2086 (1983).

³⁵ J. M. Caillol, D. Levesque, J. J. Weis and J. P. Hansen, *Jour. Stat. Phys.* **28**, 325 (1982).

³⁶ A. K. Kienappel and M. A. Moore (private communication).

This figure "figmd7.jpg" is available in "jpg" format from:

<http://arxiv.org/ps/cond-mat/9512123v2>